

A Theoretical Prediction of Regression Rates in Swirl Injection Hybrid Rocket Engines

Kohei Ozawa* and Toru Shimada**

*Department of Aeronautics and Astronautics, the University of Tokyo

3-5-1 Yoshinodai, Chuo-ku, Sagamihara, 252-5210, Japan

**Institute of Space and Astronautical Science, JAXA

3-5-1 Yoshinodai, Chuo-ku, Sagamihara, 252-5210, Japan

Abstract

In this paper, we theoretically and analytically predict what times regression rates of swirl injection hybrid rocket engines increase higher than axial injection ones by estimating heat flux from boundary layer combustion to the fuel port. We assume the schematic of engines as ones whose oxidizer is injected from the opposite side of the nozzle such as ones of Yuasa et al. propose. To simplify the estimation, we assume some hypothesis such as three dimensional axisymmetric flows. The results of this prediction method are largely consistent with Yuasa's experiments data in the range of high swirl numbers.

Nomenclature

a	: constant related to regression rate	q	: constant used for approximation of the function of blowing parameter in axial flows
B	: blowing parameter $B_z \equiv \frac{(\rho u_r)_w u_{ze}}{\tau_{zw}}$	q'	: constant used for approximation of the function of blowing parameter in swirl flows
B_θ	$\equiv \frac{(\rho u_r)_w u_{\theta e}}{\tau_{\theta w}}$	q_r	: radial direction heat flux
B_t	: thermodynamic chemical blowing parameter $B_t \equiv \frac{u_{ez} \Delta h}{u_{bz} h_v}$ (in quasi-steady condition, equal to B_z)	\dot{Q}_c	: heat flux to the wall
C	: specific heat of solid fuels	r	: radial location
C_f	: skin-friction coefficient in axial flow	\dot{r}	: regression rate
C_{f_z}	$\frac{\tau_{rzw}}{1/2 \rho u_{ze}}$	S	: swirl number
C_{f_θ}	$\frac{\tau_{r\theta w}}{1/2 \rho u_{\theta e}}$	t	: time
C_H	: Stanton number	T	: temperature
C_p	: specific heat at constant pressure	u	: velocity
D	: port diameter	z	: axial location
G_o	: oxidizer mass flux	α_z	: constant related to approximation of C_{f_z}
Δh	: enthalpy difference between flame sheet and port surface	β_z	: constant related to approximation of C_{f_z}
h_v	: total enthalpy of solid fuel gasification from ambient temperature	γ_z	: exponent related to approximation of C_{f_z}
k	: blocking exponent in axial flows	δ	: boundary layer thickness
k'	: blocking exponent in swirl flows	ε	: perturbation scale
l	: mixing length tensor	η	: nondimensional height in boundary layer
L	: port length	θ	: angle
n	: mass flux exponent for hybrids	κ	: constant related to mixing length
P	: pressure	μ	: average gas viscosity
p	: exponent related to swirl decay in cold	ν	: average gas kinematic viscosity
		ξ	: swirl strength $\frac{\xi}{2} \approx S$
		ρ	: density

τ	: shear stress	f	: fuel
φ	: nondimensional velocity in boundary layer	o	: oxidizer
ω	: angular velocity	r	: radial direction
$\bar{\omega}$: nondimensional angular velocity	ref	: reference point
	$\bar{\omega} = \frac{R - \delta_{\theta}}{u_{\theta_e}} \omega$	w	: wall
Subscripts		z	: axial direction
b	: flame area	θ	: angular direction
bl	: boundary layer	ξ	: in cases with swirl
e	: free stream or main flow	$\bar{\quad}$: nondimensionalized
		\cdot	: time differential

1. Introduction

Hybrid propulsion is expected to be applied for various purposes like space transportation, space tourism and space education because of its inherent safety and low cost. In conventional hybrid rocket engines, liquid oxidizer is injected into a combustion chamber that contains solid fuel, such as HTPB (which is a binder for solid rocket motors). Gasified oxidizer and fuel combust in the boundary layer over the fuel-port wall surface. Hybrid rockets using HTPB have been developed for many years, of which performance dead-ends because the regression rate using HTPB is low (up to 1 mm s^{-1} below the oxygen mass flux of $100 \text{ kg m}^{-2} \text{ s}^{-1}$) [1]. That is why multi-port systems are required in the practical use of hybrid engines used HTPB. However, these systems decrease launch capability from potential one because of remnants of the fuel in multi-port engines and have an anxiety of the drop of them around the end times of combustion.

To solve this problem, swirl injection (or vortex injection) method is proposed as a way to realize higher regression rates without energetic additives or the change of fuels [2] [3]. This method is to inject liquid oxidizer that has swirl velocity components. The characteristics of this injection method is that the radial pressure gradient caused by swirl makes the flame area in the boundary layer more close to the wall of the fuel port. This effect increases the amount of heat transfer from the flame area to the wall, and then, higher regression rates can be achieved. Lab-scale swirl injection hybrid rocket motors have been developed and proved that the increase of regression rates by several researchers (e.g. Yuasa [2] and Knuth [3]). However, there have been few studies which theoretically and quantitatively predict the increase of regression rates by swirl, though they will be useful for designing whatever scale of engines, for the comprehension about the phenomena in engines, and as another way to estimate the effects of swirl strength to the regression rate and other properties. Furthermore, theoretical and analytical studies have a flexibility which means that studies are not restricted by practical limitation such that a variable is originally independent on other ones, but in actual experiments, one depends on others because of the experimental equipment. For this reason, theoretical approach can reveal hidden property of a phenomenon which experimental approach cannot. Moreover, Current CFD approaches cannot always accurately simulate actual swirl flows and the techniques about swirl flows on CFD is on the way of development [4]. That is why it is significant to construct the theoretical analytical approach for the prediction of regression rates in swirl injection hybrid rockets.

The purpose of this paper is to extend the estimation method of regression rates for axial hybrid rocket engines to for swirl injection ones. To predict regression rates, we should estimate heat flux to the fuel port with some already known quantities which represent flow field and other parameters about the combustion chamber because we obtain the following equation at quasi-steady states:

$$\dot{Q}_c = \rho_f \dot{r} h_v \quad (1)$$

Because ρ_f and h_v are almost decided by fuel species and ambient temperature (h_v includes the amount of specific heat to gasify the fuel of the ambient temperature), if you have another expression of Q_c , you can estimate regression rates. In 1960s, Marxman [5] [6], and Gilbert [5] conducted theoretical and analytical studies about boundary layer combustion and evaluated heat transfer to the wall of fuels in axial hybrid motors. Their approach starts from the linkage between the heat transfer and the skin-friction by Lees [7]. This equation means that if the skin-friction with the fuel blowing from the wall can be estimated, it is possible to estimate the heat flux to the wall. Their approach to evaluate the shear stress at the wall with fuel blowing was to express it with the simple one without fuel blowing which can be express by an empirical formula.

In our study, first, we add some hypotheses which are needed to simplify the problem and to evaluate the effects of circumferential flows, we extend the flow field to three dimensional axisymmetric flows. However, the concept of

the approach to evaluate the heat flux of swirl injection hybrids is the same as the one past researchers took in the aspect of the introduction of Reynolds analogy and the connection with the shear stress at the wall. When we consider Reynolds analogy, we can understand that the temperature field is not similar to the scholar of the velocity vector but to the axial component of the velocity vector. And then, we attempt to evaluate the axial component of the shear stress at the wall in swirl flows with fuel blowing with the one without fuel blowing. On the way of the evaluation, we use flow field in boundary layer with swirl and no fuel blowing to evaluate the effects of swirl and blowing individually. Eventually, we derive the theoretical estimation of regression rates in swirl injection hybrids and compare the predicted values with experimental results of Yuasa et al. [2].

2. Modeling and hypotheses of flows in swirl injection hybrid rocket engines

First of all, we consider 10 hypotheses mainly related to the flow fields. These can largely be classified into two types. One type is the same assumptions as the theory of Marxman et al. to simplify the complex flow in chambers. Another type is newly added to handle swirl flows easily and observed in experiments related to swirl flows. The hypotheses we assumed in this paper is summarized in Table 1. These hypotheses are set for the engines whose schematics are the same type as ones Yuasa et al. proposed (Fig. 1).

Of the hypotheses of Table 1, No.1 is set to simplify flow fields. No.2, 3, 4, and 6 are the same assumptions as the theory of Marxman et al. No. 2 makes it possible to apply Reynolds analogy. No. 3 is not clearly declared but we think this hypothesis is used in their theory because Karman's momentum integral equation is used in their derivation of the friction coefficient with fuel blowing. No.4 and 5 are assumed to simplify calculating swirl numbers and because in the experimental results of Steenbergen [8] and Kito et al. [9] the flow fields similar to these hypotheses are observed around the downstream where the effects of the swirlers used are much small. The reason for applying the power law to the angular velocity with No.7 is that the definition of shear stress of the radial direction parallel to the circumferential direction is expressed as $\mu r \frac{\partial \omega}{\partial r}$. Hypothesis No.9 is assumed because of the experimental results of Steenbergen [8] and Kito et al. [9] and for simplification of the problem. In all their results, the axial component of the boundary layer thickness is larger than the circumferential one around the downstream where the effects of the swirlers used in these experiments are much small. No. 10 is set to simplify the flow field and some researchers such as Karabeyoglu et al. [10] adopted this assumption for this reason. However, we think this assumption is not always suitable if metal or carbon powders are added to increase radiation or absorption of it during combustion.

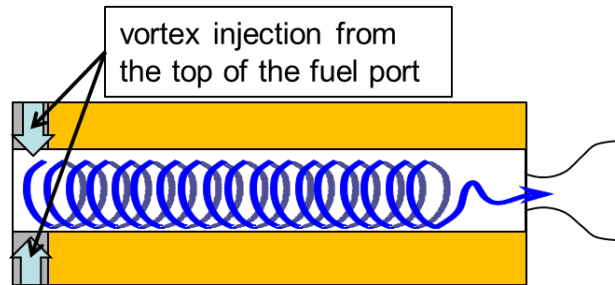


Figure 1: The schematics of swirl injection hybrid rocket engines we consider in this paper.

Table 1: The hypotheses on swirl flows

1.	The flow in the combustion chamber is axisymmetric.
2.	The Prandtl number in the flow is 1.
3.	The flow in the boundary layer is incompressible.
4.	Axial velocity components are uniform to the axial and radial directions except in the boundary layer over the fuel-port wall surface.
5.	Circumferential velocity distribution is the same as rigid body rotation to the radial direction except in the boundary layer over the fuel-port wall surface.

6.	Axial velocity components in the boundary layer obey the power law when there is not blowing from the solid fuel.
7.	Circumferential angular velocity components in the boundary layer obey the power law when there is no blowing from the solid fuel.
8.	The swirl without fuel blowing from the solid fuel decays exponentially to the axial direction.
9.	The axial boundary layer thickness is larger than the circumferential one.
10.	The heat flux to the fuel port by heat convection is much larger than the one by radiation.

3. The Derivation of regression rates in swirl injection hybrid rocket engines

In this section, we aim to derive the equation to estimate regression rates in swirl injection hybrid rocket motors theoretically on the basis of the hypotheses in the last section. Because regression rates are linked with the heat flux to the wall through the energy conservation Eq. (1), in order to derive regression rates with the variables of swirl flows, we should express the heat flux to the wall in the aspect of fluid dynamics and combustion. Therefore, first, in the same way as Marxman et al., we attempt to relate the axial velocity field with the temperature field through Reynolds analogy which is extended from Lees's model in two dimensional coordinates to the model in axisymmetric three dimensional coordinates. Because each radial partial differential of them is proportional to the axial components of shear stress and heat flux respectively, we can express heat flux with variables about the flow in the combustion chamber. (Fig. 2) Next, we attempt to express the axial shear stress with the scale of motors, axial position, thermochemical and mechanical parameters of propellants, and the boundary conditions related to flows in the engines such as the swirl strength at the injectors, the axial velocity and Reynolds number in the main flow. In the process of the derivation of the axial shear stress at the wall, we newly introduce four boundary layer models. Three of the four models are respectively different turbulent models in the boundary layer and the last one is Karman's momentum integral equation. Our approach of this process is also the same as the one of Marxman et al., namely, which is to multiply the correction terms to the skin-friction coefficient in the flat plate boundary layer without fuel blowing. The correction terms mean the effects of fuel blowing and swirl injection and they are separately derived. Finally, the combination of this expression with Eq. (1) and the empirical rule of the skin-friction coefficient in two dimensional flat plate boundary layer without fuel blowing makes it possible to derive regression rates of the swirl injection engines.

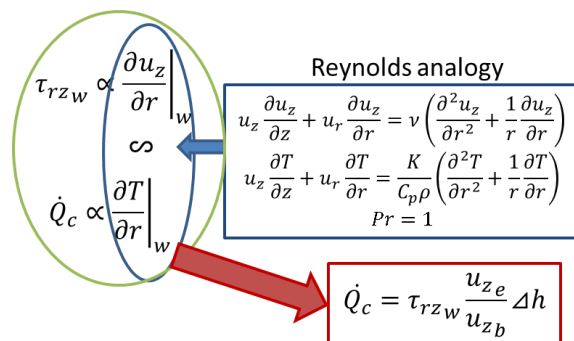


Figure 2: Reynolds analogy

3.1 Reynolds analogy

Reynolds analogy means the similarity of the velocity boundary layer to the thermal boundary layer. This analogy holds because the effect of axial partial differentials in both viscosity and pressure terms is much smaller than radial partial differentials and can be ignored in boundary layers. We extend this analogy to the three dimensional axisymmetric coordinates.

We compare the momentum equation with the energy conservation equation. The axial component of the momentum equations can be written as

$$u_z \frac{\partial u_z}{\partial z} + u_r \frac{\partial u_z}{\partial r} = \nu \left(\frac{\partial^2 u_z}{\partial r^2} + \frac{1}{r} \frac{\partial u_z}{\partial r} \right) \quad (2)$$

where we have used the hypothesis No. 1 and assumed that the axial gradients of shear stress and pressure is much smaller than the radial ones as an approximation which can commonly be used in the boundary layer. The energy conservation law can be written as

$$u_z \frac{\partial T}{\partial z} + u_r \frac{\partial T}{\partial r} = \frac{K}{c_p \rho} \left(\frac{\partial^2 T}{\partial r^2} + \frac{1}{r} \frac{\partial T}{\partial r} \right) \quad (3)$$

where we have assumed the effect of the heat derived from viscosity can be ignored because the convection heat transfer, which comes from flame, in other words, from outside of a piece of a microvolume in the boundary layer, is much greater than frictional heat generated within it. By the assumption that Prandtl number is 1 (hypothesis No. 2), we can use Reynolds analogy and relate the temperature distribution with velocity distribution in the boundary layer. We can consider the radial distribution of u_z is similar to the one of T in the boundary layer. This similarity can be expressed as follows

$$\frac{du_z}{u_{zb} - u_z} = \frac{dT}{T_b - T} \quad (4)$$

Then, the heat flux to the wall is linked with the shear force stress at the wall because temperature axial differential at the wall is proportional to the heat flux to the wall and the velocity one is proportional to the shear stress at the wall. The difference between the scales of the axial and radial differential yields following approximations as

$$du_z \approx \frac{\tau_{rz}}{\mu} dr \quad (5.a)$$

$$dT \approx -\frac{q_r}{K} dr \quad (5.b)$$

Eq. (4), (5.a) and (5.b) yields

$$h \equiv -\frac{q_{rw}}{T_b - T_w} = \frac{c_p \tau_{rzw}}{u_{zb}} \quad (6)$$

From the definition of Stanton numbers and Eq. (6), the following equation can be derived as

$$C_H \equiv \frac{h}{c_p \rho u_b} = \frac{\tau_{rzw}}{\rho_b u_b} \quad (7)$$

Here, we define the following nondimensional axial skin-friction parameter we call ‘‘axial skin-friction coefficient’’ for the convenience of the subsequent calculations as

$$\frac{C_{fz}}{2} \equiv -\frac{\tau_{rzw}}{\rho_e u_{ze}^2} \left(= -\frac{\tau_{zw}}{\rho_e u_{ze}^2} \right) \quad (8)$$

where the reason why we put minus sign on the middle and right hand of Eq. (8) is that the shear stress at the wall is always minus. Therefore, the heat flux to the wall can be written as

$$\dot{Q}_c = C_H \rho_b u_b \Delta h = \frac{C_{fz} \rho_e u_{ze}^2}{2 u_{bz}} \Delta h \quad (9)$$

Here, we should focus on the right side of Eq. (9). In this expression, there is no variable related to circumferential components. Considering the fact that the circumferential energetic balance is zero because of axisymmetric flows, this result is reasonable. Then, we can expect that the axial friction coefficient should be only affected by swirl because we also maintain the hypothesis by Marxman et al. that the remained components except the axial friction coefficient are regarded as the constants that are mainly determined by ambient temperature and chemical species and phases of fuel and oxidizer used in a motor [11]. Therefore, in the next section, we attempt to express the axial

skin-friction coefficient with axial distance, mass flux, swirl number, scale of the motor, or other variables determined in advance.

3.2 Turbulent flow models

Next, we must express the axial skin-friction coefficient with other parameters we can know in advance. The first one of three different turbulent stress models is the Prandtl's mixing length theory extended to three-dimension by Czernuszenko and Rylov [12]. If each eigenvector of the mixing length tensor is parallel to each cylinder coordinate axis and the all norms of the eigenvectors are the same, the axial component of the shear stress including Reynolds stress are expressed as

$$\tau_{rz} \approx \left\{ \mu + \rho l^2 \left(\left| \frac{\partial \bar{u}_\theta}{\partial r} - \frac{\bar{u}_\theta}{r} \right| + \left| \frac{\partial \bar{u}_z}{\partial r} \right| \right) \right\} \frac{\partial \bar{u}_z}{\partial r} \quad (8)$$

where we have assumed the circumferential partial differentials are much larger than the axial ones.

The second one comes from the extended expression of the boundary layer theory on vaporing surface from flat plate in two dimensional coordinates by Dorance and Dore [13] to three dimensional axisymmetric flows as

$$\tau_{rz} \approx \tau_{rzw} (1 + B_z \varphi_z) \quad (9.a)$$

$$\tau_{r\theta} \approx \tau_{r\theta w} (1 + B_\theta \varphi_\theta) \quad (9.b)$$

where we have assumed that the boundary layer thickness is much thinner than the port radius. The definition of B_z and B_θ are $B_z \equiv \frac{(\rho u_r)_w u_{ze}}{\tau_{zw}}$ and $B_\theta \equiv \frac{(\rho u_r)_w u_{\theta e}}{\tau_{\theta w}}$ respectively. Eq. (9.a) and (9.b) is derived by evaluating Reynolds stress and blowing in the same way as they did in the flat plate. Note that B_z is a constant throughout the fuel port but B_θ is not. The reason for this treatment is accounted for the section 3.6.

Now, we have already introduced two of three turbulent models. From now on, we manipulate these equations and evaluate the velocity distribution and the axial skin-friction coefficient. Combining Eq. (8) with (9.a) yields

$$\tau_{rzw} (1 + B_z \varphi_z) = \left\{ \mu + \rho l^2 \left(\left| \frac{\partial \bar{u}_\theta}{\partial r} - \frac{\bar{u}_\theta}{r} \right| + \left| \frac{\partial \bar{u}_z}{\partial r} \right| \right) \right\} \frac{\partial \bar{u}_z}{\partial r} \quad (10)$$

Here the power law in cases of no fuel vaporization (hypotheses No. 6 and 7) is written as

$$\varphi_z = \eta_z^{n_z} \quad (11.a)$$

$$\bar{\omega} = \eta_\theta^{n_\theta} \quad (11.b)$$

where we set $n_z = n_\theta = 1/7$.

Applying Eq. (11.a) and (11.b) to the absolute values of the velocity partial differentials in Eq. (10) yields

$$\frac{c_{f_z} u_{ze} (R - \delta_\theta)}{2 \kappa^2 n_\theta \delta_z u_{\theta e}} (1 + B_z \varphi_z) = \left\{ \eta_z^2 - \frac{R - \delta_\theta}{\delta_z} \left(1 + \frac{n_z u_{ze}}{n_\theta u_{\theta e}} \right) \eta_z - \frac{u_{ze} (R - \delta_\theta)}{\kappa^2 Re_{\delta_z} n_\theta \delta_z u_{\theta e}} \right\} \frac{\partial \varphi_z}{\partial \eta_z} \quad (12)$$

where we have used $l = \kappa(R - r)$ and $\kappa = 0.4$.

Eq.(12) can be integrated to the radial direction from the edge of the boundary layer to the fuel port wall. This integration yields

$$\frac{c_{f_z}}{2} \approx \frac{\kappa^2 (n_\theta \frac{u_{\theta e}}{u_{ze}} + n_z)}{\ln \{ 1 + \kappa^2 Re_{\delta_z} (n_\theta \frac{u_{\theta e}}{u_{ze}} + n_z) \}} \frac{\ln(1 + B_z)}{B_z} \quad (13)$$

where we have approximated $R \gg \delta_z, \delta_\theta$ and $\kappa^2 Re_{\delta_z} n_\theta \gg 1$. The first term in the right side of Eq. (13) can be approximated in the easier way as

$$\frac{c_{f_z}}{2} = (\alpha_z \xi + \beta_z) Re_{\delta_z} \gamma_z \frac{\ln(1 + B_z)}{B_z} \quad (14)$$

where we set $(\alpha_z, \beta_z, \gamma_z) = (0.00769, 0.0233, -0.125)$. We call $\xi \equiv u_{\theta e}/u_{ze}$ “swirl strength”. If $\xi = 0$, Eq. (14) becomes the same form as Marxman’s approximation [6].

Though the axial skin-friction coefficient has been written as Eq. (14) with variables which show the properties of the flows, in Eq. (14), there are three variables we cannot easily know: ξ , u_{ze} , δ_z . Therefore, we need three other constraint conditions.

The first one is Boussinesq approximation and this is the third of the three turbulent models as follows

$$\tau_{rz} = (\mu + \rho\varepsilon) \frac{u_{ze}}{\delta_z} \frac{\partial \varphi_z}{\partial \eta_z} \quad (15.a)$$

$$\tau_{r\theta} = (\mu + \rho\varepsilon) \frac{u_{\theta e}}{\delta_\theta} \frac{\partial \varphi_\theta}{\partial \eta_\theta} \quad (15.b)$$

Applying Eq. (15.a) and (15.b) to Eq. (9.a) and (9.b) yield

$$\frac{\tau_{rz} \delta_z}{(\mu + \rho\varepsilon) u_{ze}} (1 + B_z \varphi_z) = \frac{\partial \varphi_z}{\partial \eta_z} \quad (16.a)$$

$$\frac{\tau_{r\theta} \delta_\theta}{(\mu + \rho\varepsilon) u_{\theta e}} (1 + B_\theta \varphi_\theta) = \frac{\partial \varphi_\theta}{\partial \eta_\theta} \quad (16.b)$$

Here, we assume that $\frac{\tau_{rz} \delta_z}{(\mu + \rho\varepsilon) u_{ze}}$ consists of the product of two single variable functions which is the function of η_z and B_z respectively in the same way as Marxman’s [5]. In the cases of no blowing, Eq. (16.a) and (16.b) is equivalent to the derivative-type of Eq. (11.a) and (11.b). Moreover, we approximate $1 + B_z \varphi_z \approx 1 + B_z \eta_z^{n_z}$ because of the hypothesis No. 6. Therefore, we can express (16.a) as

$$\frac{\partial \varphi_z}{\partial \eta_z} = F(B_z) n_z \eta_z^{n_z-1} (1 + B_z \eta_z^{n_z}) \quad (17)$$

Eq. (17) can be integrated to the radial direction from the edge of the boundary layer to the fuel port wall. Considering boundary conditions of $\varphi_z(\eta_z = 0) = 0$ and $\varphi_z(\eta_z = 1) = 1$, we lead

$$\varphi_z = \frac{\eta_z^{n_z} (1 + \frac{B_z}{2} \eta_z^{n_z})}{1 + \frac{B_z}{2}} \quad (18.a)$$

About circumferential direction, in the same way as the derivation of Eq. (18.a), we can derive

$$\bar{\omega} = \frac{\eta_\theta^{n_\theta} (1 + \frac{B_\theta}{2} \eta_\theta^{n_\theta})}{1 + \frac{B_\theta}{2}} \quad (18.b)$$

where we have assumed $R \gg \delta_z, \delta_\theta$.

Now, we have evaluated the velocity fields to the radial direction in the boundary layer. These equations are used in two situations. One of them is the cases where we compare shear stress between with fuel blowing and with no blowing. Another one is the cases where we unite Eq. (14), (18.a), and (18.b) to the Karman’s momentum integral equation and derive the axial skin-friction coefficient as a function of axial position.

3.3 Karman’s momentum integral equation

Next, we derive the Karman’s momentum integral equation in the axisymmetric pipe flow as the second condition to eliminate an unknown variable of Eq. (14). We show the mass conservation law and the momentum conservation law:

Mass conservation law

$$\frac{\partial u_z}{\partial z} + \frac{\partial u_r}{\partial r} + \frac{u_r}{r} = 0 \quad (19)$$

Momentum conservation law

$$u_z \frac{\partial u_z}{\partial z} + u_r \frac{\partial u_z}{\partial r} = -\frac{1}{\rho} \frac{\partial P}{\partial z} + \nu \left(\frac{\partial^2 u_z}{\partial r^2} + \frac{1}{r} \frac{\partial u_z}{\partial r} \right) \quad (20.a)$$

$$\frac{u_\theta^2}{r} = -\frac{1}{\rho} \frac{\partial P}{\partial r} \quad (20.b)$$

$$u_z \frac{\partial u_\theta}{\partial z} + u_r \frac{\partial u_\theta}{\partial r} + \frac{u_r u_\theta}{r} = \nu \left(\frac{\partial^2 u_\theta}{\partial r^2} + \frac{1}{r} \frac{\partial u_\theta}{\partial r} - \frac{u_\theta}{r^2} \right) \quad (20.c)$$

where we have ignored axial partial differentials in viscous terms. Eq. (19) $\times r u_z$ + Eq. (20.a) $\times r$ and the partial integration of Eq. (19) yield the momentum integral as

$$\frac{\partial}{\partial z} \int_R^{R-\delta_z} r u_z^2 dr - u_{ze} \frac{\partial}{\partial z} \int_R^{R-\delta_z} r u_z dr = -\frac{R\tau_{rzw}}{\rho} (1 + B_z) - \frac{\partial}{\partial z} \int_R^{R-\delta_z} \frac{rP}{\rho} dr \quad (21)$$

where note that we must consider $(\rho u_r)_w$ as a non-zero variable. In axial flows, $\frac{\partial}{\partial z} \left(\frac{rP}{\rho} \right)$ can be shown with the velocity of main flows by concerning the edge of boundary layer because $\frac{\partial P}{\partial r}$ is approximated 0. However, in swirl flows, this assumption cannot be used because of Eq. (20.b). Thus, we must newly consider the method of evaluation of the pressure gradient $\frac{\partial}{\partial z} \left(\frac{rP}{\rho} \right)$. Now, the pressure in the boundary layer can be expressed as

$$P(z, r) = P(z, R - \delta_z) + \int_{R-\delta_z}^r \frac{\partial P}{\partial r} dr = P(z, R - \delta_z) - \int_{R-\delta_z}^r \rho \frac{u_\theta^2}{r} dr \quad (22)$$

Applying Eq. (22) to the second term in the right side of the Eq. (21) leads

$$\frac{\partial}{\partial z} \int_R^{R-\delta_z} \frac{rP}{\rho} dr = \int_R^{R-\delta_z} r \left(\frac{1}{\rho} \frac{\partial P}{\partial z} \Big|_{R-\delta_z} - \frac{\partial}{\partial z} \int_{R-\delta_z}^r \frac{u_\theta^2}{r} dr \right) dr \quad (23)$$

The hypothesis No. 4 and Eq. (21) in the case of the edge of the boundary layer yield

$$\frac{\partial P}{\partial z} \Big|_{R-\delta_z} = 0 \quad (24)$$

Because of the hypothesis No. 9, we can divide the last term of Eq. (23) and evaluate it as

$$\begin{aligned} & - \int_R^{R-\delta_z} \left(r \frac{\partial}{\partial z} \int_{R-\delta_z}^r \frac{u_\theta^2}{r} dr \right) dr \\ = & - \frac{\partial}{\partial z} \int_{R-\delta_\theta}^{R-\delta_z} r \left(\int_{R-\delta_z}^r \frac{u_\theta^2}{r} dr \right) dr - \frac{\partial}{\partial z} \int_R^{R-\delta_z} r \left(\int_{R-\delta_z}^{R-\delta_\theta} \frac{u_\theta^2}{r} dr \right) dr - \frac{\partial}{\partial z} \int_R^{R-\delta_\theta} r \left(\int_{R-\delta_\theta}^r \frac{u_\theta^2}{r} dr \right) dr \quad (25) \\ \approx & \frac{1}{2} \frac{\partial}{\partial z} \{ R^2 \omega_e^2 (\delta_z^2 - \delta_\theta^2) \} + \frac{\partial}{\partial z} \left\{ \frac{49(170B_\theta^2 + 792B_\theta + 935)R^2 \omega_e^2 \delta_\theta^2}{33660(B_\theta + 2)^2} \right\} \end{aligned}$$

where the last expression of Eq. (25) is approximated in the way that the terms of the largest order of magnitude are only taken from the precise answer. Applying Eq. (24) and (25) to Eq. (21) and nondimensionalization yields

$$\frac{7(40B_z^2 + 143B_z + 110)}{1980(B_z + 2)^2} \frac{\partial \delta_z}{\partial z} \approx \frac{C_{fz}}{2} (1 + B_z) + \frac{1}{2} \frac{\partial}{\partial z} \left\{ \xi^2 \frac{\delta_z^2 - \delta_\theta^2}{R \left(1 - \frac{\delta_\theta}{R} \right)^2} \right\} + \frac{\partial}{\partial z} \left\{ \frac{49(170B_\theta^2 + 792B_\theta + 935)\xi^2 \delta_\theta^2}{33660(B_\theta + 2)^2 R \left(1 - \frac{\delta_\theta}{R} \right)^2} \right\} \quad (26)$$

Because the order of magnitude of the last two terms in the right side of Eq. (26) is $\frac{\delta^2}{RL}$ and it is much smaller than the one of the right side, which is $\frac{\delta}{L}$, we can approximate Eq. (26) as

$$\frac{7(40B_z^2 + 143B_z + 110)}{1980(B_z + 2)^2} \frac{\partial \delta_z}{\partial z} \approx \frac{C_{fz}}{2} (1 + B_z) \quad (27)$$

This is Karman's momentum integral equation in the three dimensional axisymmetric coordinates. This equation is the last one of the four models related to boundary layers.

3.4 Estimation of the axial skin-friction coefficient in swirl flows with no blowing

In this section, we aim to show the last condition of three conditions needed to evaluate the axial skin-friction coefficient and we attempt to evaluate the rate of it in case of swirl flow and no blowing to the one in the cases of axial flow and no blowing.

Before we introduce the last condition related to swirl decay, we must define the indicator which shows swirl strength. Swirl number is a way to express it as follows

$$S \equiv 2 \frac{\int_0^R r^2 u_z u_\theta dr}{R^3 u_z^2} \quad (28)$$

Considering the hypotheses No. 4 and 5, Ignoring boundary layers and rough calculation yields

$$S \approx \frac{\xi}{2} \quad (29)$$

Here, we call ξ ‘‘swirl strength’’. The last condition is the hypothesis No. 8 and the mathematical description of this is

$$S \approx S_0 \exp(pz) \text{ or } \xi \approx \xi_0 \exp(pz) \quad (28)$$

where $p = -0.569 \times Re_D^{-0.277} D^{-1}$ and these equations are empirically derived from Steenbergen’s research [8] and Kito’s research [9].

Now, we have assembled necessary and sufficient conditions, which are Eq. (18.a), (18.b), (27), and (28), to rewrite Eq. (14) as a single variable function of axial direction. Next, we aim to compare and evaluate C_{f_z} with the one without blowing and swirling, namely, we evaluate C_{f_z} as

$$\frac{C_{f_z}}{2} \Big|_{B_z, \xi_0} = \frac{C_{f_z} \Big|_{B_z, \xi_0}}{C_{f_z} \Big|_{B_z=0, \xi_0}} \frac{C_{f_z} \Big|_{B_z=0, \xi_0}}{C_{f_z} \Big|_{B_z=0, \xi_0=0}} \frac{C_{f_z}}{2} \Big|_{B_z=0, \xi_0=0} \quad (29)$$

where $\frac{C_{f_z}}{2} \Big|_{B_z=0, \xi_0=0}$ is equivalent to $\frac{C_f}{2}$ in cases of two dimensional flat plate and $\frac{C_f}{2}$ has a famous and empirical rule as follows

$$\frac{C_f}{2} = 0.03 Re_z^{-0.2} \quad (30)$$

In this section, we will evaluate $C_{f_z} \Big|_{B_z=0, \xi_0} / C_{f_z} \Big|_{B_z=0, \xi_0=0}$ with initial swirl strength and axial direction. Now, in the cases with no blowing, substituting Eq. (14) and (29) for Eq. (27) and integration of Eq. (27) to the axial direction from 0 to z yield

$$\bar{\delta}_z \Big|_{B_z=0} = \left\{ \frac{72(1-\gamma z)}{7} \right\}^{\frac{1}{1-\gamma z}} Re_D (\alpha_z \xi_0 \frac{\exp(\bar{p}\bar{z})-1}{\bar{p}} + \beta_z \bar{z})^{\frac{1}{1-\gamma z}} \quad (31)$$

where the bar means that the variable is nondimensionalized by the port diameter. By substituting Eq. (31) for Eq. (27) and dividing Eq. (27) with swirl by the one without swirl, we can obtain

$$\frac{C_{f_z} \Big|_{B_z=0, \xi_0}}{C_{f_z} \Big|_{B_z=0, \xi_0=0}} = \frac{C_{f_z} / 2 \Big|_{B_z=0, \xi_0}}{C_f / 2} = \left(\frac{\alpha_z}{\beta_z} \xi_0 \frac{\exp(\bar{p}\bar{z})-1}{\bar{p}} + 1 \right)^{\frac{1}{1-\gamma z}} \left(\frac{\alpha_z}{\beta_z} \xi_0 \exp(\bar{p}\bar{z}) + 1 \right) \quad (32)$$

Eq. (32) shows the relation between the axial skin-friction coefficient with swirl and without fuel blowing. This evaluation is used in subsequent sections.

3.5 Estimation of the axial friction coefficient in swirl flows with blowing

In this section, we start from the comparison of shear stresses between whether there is fuel blowing, and then, we express boundary layer thickness and the axial skin-friction coefficient with fuel blowing and axial blowing parameter.

First of all, we write the shear stress at the wall with fuel blowing as

$$\tau_{rzw}|_{B_z} = \mu \frac{u_{ze}}{\delta_z|_{B_z}} \frac{\partial \varphi_z}{\partial \eta_z} \Big|_w \quad (33)$$

Near the wall, nondimensional axial velocity is approximated as follows

$$\varphi_z = \frac{\eta_z^{n_z} \left(1 + \frac{B_z}{2} \eta_z^{n_z}\right)}{1 + \frac{B_z}{2}} \approx \frac{\eta_z^{n_z}}{1 + \frac{B_z}{2}} \quad (34)$$

Substituting Eq. (34) for Eq. (33) yields

$$\tau_{rzw}|_{B_z} \approx \frac{\mu}{1 + \frac{B_z}{2}} \frac{u_{ze}}{\delta_z|_{B_z}} \frac{\partial \eta_z^{n_z}}{\partial \eta_z} \Big|_w = \frac{1}{1 + \frac{B_z}{2}} \frac{\delta_z|_{B_z=0}}{\delta_z|_{B_z}} \tau_{rzw}|_{B_z=0} \quad (35)$$

Therefore, we can nondimensionalize Eq. (35) as

$$\frac{c_{f_z}}{2} \Big|_{B_z} = \frac{1}{1 + \frac{B_z}{2}} \frac{\delta_z|_{B_z=0}}{\delta_z|_{B_z}} \frac{c_{f_z}}{2} \Big|_{B_z=0} \quad (36)$$

Applying Eq. (27) to the both sides of Eq. (36) and integration to the axial distance yield Eq.(37) as

$$\delta_z|_{B_z} = \sqrt{\frac{(1+B_z)(1+B_z/2)}{1+13/11B_z+4/11B_z^2}} \delta_z|_{B_z=0} \quad (37)$$

By substituting Eq.(37) for Eq. (27) and approximation of B_z in the range from 2 to 50, we can obtain

$$\frac{c_{f_z}|_{B_z}}{c_{f_z}|_{B_z=0}} = \frac{1}{(1+B_z/2)} \sqrt{\frac{1+13/11B_z+4/11B_z^2}{(1+B_z)(1+B_z/2)}} \approx q' B_z^{-k'} \quad (38)$$

where we have set $(q', k') = (0.7275, 0.965)$.

By combining Eq. (29) with Eq. (30), (32), and (38) we can evaluate the axial skin-friction coefficient as

$$\frac{c_{f_z}}{2} \Big|_{B_z} = \left(\frac{\alpha_z}{\beta_z} \xi_0 \frac{\exp(\bar{p}\bar{z})-1}{\bar{p}\bar{z}} + 1 \right)^{\frac{1}{1-\gamma_z}} \left(\frac{\alpha_z}{\beta_z} \xi_0 \exp(\bar{p}\bar{z}) + 1 \right) q' B_z^{-k'} 0.03 Re_z^{-0.2} \quad (39)$$

3.6 The Derivation of regression rates in swirl injection engines

In the previous section, we have derived the axial skin-friction coefficient on condition that there is swirl and fuel blowing as Eq. (39). In this section, we aim to obtain heat flux to the wall and regression rates in swirl hybrids. Now, substituting Eq. (9) for Eq. (39) yields

$$\dot{Q}_c = (0.03q')^{\frac{1}{1-k'}} \rho_f^{-\frac{k'}{1-k'}} \Delta h \frac{u_{ze}}{u_{zb}} \left(\frac{z}{\mu}\right)^{-\frac{0.2}{1-k'}} \left(1 + \frac{\alpha_z}{\beta_z} \xi_0 \frac{\exp(pz)-1}{pz}\right)^{\frac{\gamma_z}{(1-\gamma_z)(1-k')}} \left\{1 + \frac{\alpha_z}{\beta_z} \xi_0 \exp(pz)\right\}^{\frac{1}{1-k'}} G_{z0}^{\frac{0.8}{1-k'}} \dot{r}^{-\frac{k'}{1-k'}} \quad (40)$$

where we have eliminated B_z with the definition of B_z and Eq. (39).

Substituting Eq. (40) for Eq. (1) yields

$$\dot{r} = \left(1 + \frac{\alpha_z}{\beta_z} \xi_0 \frac{\exp(pz)-1}{pz}\right)^{\frac{\gamma_z}{1-\gamma_z}} \left\{1 + \frac{\alpha_z}{\beta_z} \xi_0 \exp(pz)\right\} 0.03q' \left(\frac{z}{\mu}\right)^{-0.2} \rho_f^{-1} B_t^{1-k'} G_{z0}^{0.8} \quad (41)$$

where the definition of B_t is $B_t \equiv \frac{u_{ez} \Delta h}{u_{bz} h_v}$ and B_t is equivalent to B_z at quasi-steady states because of Eq. (1) and (9).

Because B_t is a function of the thermochemical properties and O/F [11], if O/F is constant, B_t is constant to the axial and radial direction. This is the reason why we consider B_θ as a variable and B_z as a constant.

According to the results by Marxman et al. [11], the heat flux to the wall can be expressed as follows

$$\dot{Q}_c = (0.03q)^{\frac{1}{1-k}} \rho_f^{-\frac{k}{1-k}} \Delta h \frac{u_e}{u_b} \left(\frac{z}{\mu}\right)^{-\frac{0.2}{1-k}} G_o^{\frac{0.8}{1-k}} \dot{r}^{-\frac{k}{1-k}} \quad (42)$$

Therefore, Eq. (1) and Eq. (42) yield

$$\dot{r} = 0.03q \left(\frac{z}{\mu}\right)^{-0.2} \rho_f^{-1} B_t^{1-k} G_o^{0.8} \quad (43)$$

Here, note that the experimental law about regression rates as follows

$$\dot{r} = aG_o^n \quad (44)$$

By Karabeyoglu's theory [14], in axial flows, averaging Eq. (43) in axial direction is equivalent to Eq. (44) and the exponent 0.8 on G_o in Eq. (43) should correspond to the exponent n on G_o in Eq. (44). On the basis of these correspondences, the coefficient a in Eq. (48) should be

$$a_0 = 0.03q \left(\frac{z}{\mu}\right)^{-0.2} \rho_f^{-1} B_t^{1-k} \quad (45)$$

where a is replaced by a_0 and $(q, k) = (1.2, 0.77)$ [6]. Then, in the same way as Eq. (45), a in Eq. (41) should be

$$a_\xi = \left(1 + \frac{\alpha_z}{\beta_z} \xi_0 \frac{\exp(pz)-1}{pz}\right)^{\frac{\gamma_z}{1-\gamma_z}} \left\{1 + \frac{\alpha_z}{\beta_z} \xi_0 \exp(pz)\right\} 0.03q' \left(\frac{z}{\mu}\right)^{-0.2} \rho_f^{-1} B_t^{1-k'} \quad (46)$$

where a is replaced by a_ξ . Then, the rate of these two coefficients shows how regression rates rise by the initial swirl strength ξ_0 as

$$\frac{\dot{r}_\xi}{\dot{r}_0} = \frac{a_\xi}{a_0} = \left(1 + \frac{\alpha_z}{\beta_z} \xi_0 \frac{\exp(pz)-1}{pz}\right)^{\frac{\gamma_z}{1-\gamma_z}} \left\{1 + \frac{\alpha_z}{\beta_z} \xi_0 \exp(pz)\right\} \frac{q'}{q} B_t^{k-k'} \quad (47)$$

Thus, we have estimated the heat flux to the wall and regression rates in swirl flows.

4. The Comparison of the regression rates of swirl engines with the experiments

In order to validate this prediction model, we can compare the increase rate by swirl between Eq. (47) and the experiments by Yuasa et al. [2]. In this chapter, we compare the prediction from Eq. (47) with experiments from the two aspects. One of them is the comparison between the representative regression rates of the predictions to the axial direction and space averaged values of the experimental results. Another one is about the axial distribution of regression rates.

4.1 The comparison of the representative and averaged regression rates to the axial distance

The fuel and oxidizer used in Yuasa's experiments are PMMA and GOX. We set $B_t = 10$ for PMMA [15] and $\mu = 5.0 \times 10^{-7}$ Pa s. To compare our prediction with the averaged data, we set the representative axial location in Eq. (47) as $L/2$. The geometric swirl numbers of the injectors are 0, 9.7, and 19.4 and the range of the oxidizer mass flux is from 10 to 70 kg m⁻² s⁻¹. The cases of the port length $L=150$ mm are shown in Fig. 3 and ones of $L=500$ mm are shown in Fig. 4.

In Yuasa's experiments, they said it was too difficult to measure the actual swirl numbers in their motors and when they plotted the regression rates, they used a kind of index called geometric swirl number as how strong the swirl was. This index is determined only by the geometry of engines and injectors and we think this number is not always equal to the actual swirl number. Actually, Motoe et al. [16] conducted numerical simulations about the swirl cold flow field where they used the shape or geometry of the chamber similar to Yuasa's. The calculated swirl numbers near the injectors are the 66% of the geometric swirl number. For this reason, we plotted regression rate in Yuasa's experiment with error bar to the swirl number direction. The error bars have the range of the 66% to 100% of the geometry swirl numbers.

Note that in both port lengths, in large swirl numbers, the increase rates of regression rates are largely consistent with the experiments and the positive correlation between initial swirl numbers and the increase rates of regression

rates also commonly exists in the set of experimental results and our prediction. In our past research, because we assumed that the decay of swirl and the axial skin-friction are not affected by fuel blowing, the increase rate was estimated to be much larger than the experimental data [17]. In this paper, we have reconsidered that assumption and assessed that it does not reflect the actual physical phenomena because the swirl decay is mainly caused by skin-friction at the wall and fuel blowing should strongly affect it. Then, we have newly considered the methods to evaluate the skin friction with fuel blowing and these approaches used in 3.4 and 3.5 have succeeded better than the past one. Then, we have successfully evaluated the regression rates in cases of strong swirl.

However, in the range of small swirl numbers under 3, the rates of regression rates are less than 1. This seems to be because, though we should have solved momentum, angular momentum, and energy coupled differential equations, in our model, in order to simplify the problem, we have assumed the exponential decay of swirl in cold flows and the separate considerations of the effects of swirl flows and fuel blowing to the skin-friction coefficient. However, when applying vortex injection to hybrids, initial swirl numbers will be highly designed to increase regression rates and we think that this estimation method seems to be useful.

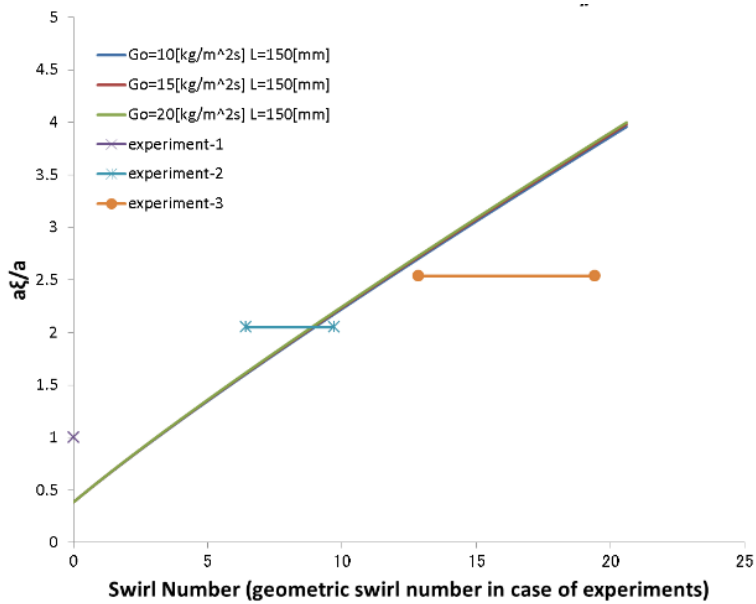


Fig. 3. The ratio of the constant “a” in swirl hybrid rocket engines in the case of L=150[mm].

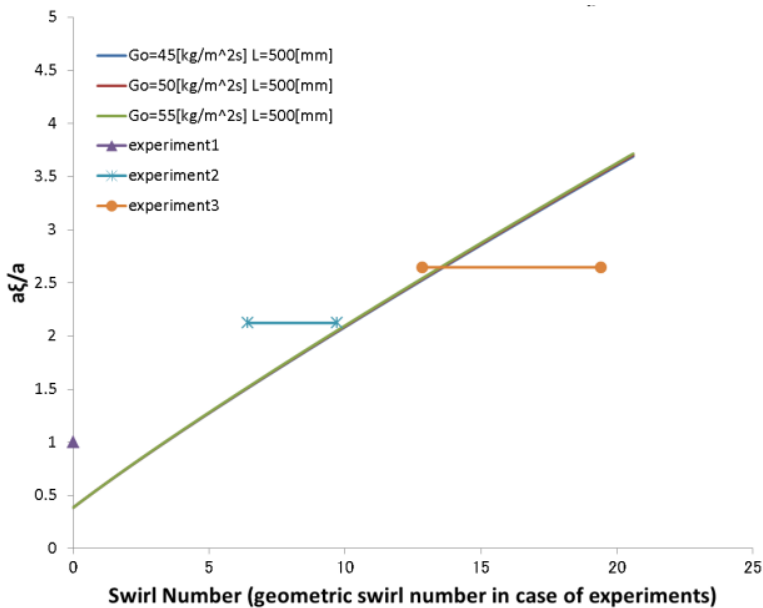


Fig. 4. The ratio of the constant “a” in swirl hybrid rocket engines in the case of L=500[mm].

4.2 The comparison of the axial distribution of regression rates

Next, we aim to compare the prediction of the local regression rates of the swirl injection hybrids with the experiments conducted by Yuasa et al. The geometric swirl numbers of the injectors are 0, 9.7, and 19.4 and the axial location where the local regression rates is measured is from 30 to 500 mm and oxidizer mass flux is $56.9 \text{ kg m}^{-2} \text{ s}^{-1}$.

Fig. 5 shows the comparison of the local regression rate in axial injection between the prediction by Eq. (43) and the experimental result. In the experimental data, while the local regression rate decreases from the front edge of the fuel port to the middle of the fuel port and increase to the end, the predicted regression rate by Marxman's evaluation constantly decreases through all the axial location. Furthermore, the location where the prediction agrees with the experimental data is only around the local minimum position. We think this disagreement suggests that other effects which increase regression rates such as radiation and the increase of the mass flux by fuel blowing have to be considered.

In Fig. 6, the prediction of the local regression rates by Eq. (41) is compared with Yuasa's experiments of the swirl injection hybrid mortars. Similar to the case of axial injection, while both predicted regression rates and experimental results are the same order of magnitude in the high swirl numbers, their values are not the same. As is the case in the comparison of averaged rates, especially in low swirl numbers, the prediction is much separated from the experimental data because Eq. (47) takes values under 1.

Because the theoretical accuracy of the regression rate prediction in axial injection hybrids is not enough, even if we observe Fig.6 cautiously, the improvement of our model will be difficult. We think that, about the axial distribution of the regression rates, before we start to focus on improving the evaluation of the effects by swirl injection, it is important to attempt to improve the prediction of the local regression rates distribution in axial flows.

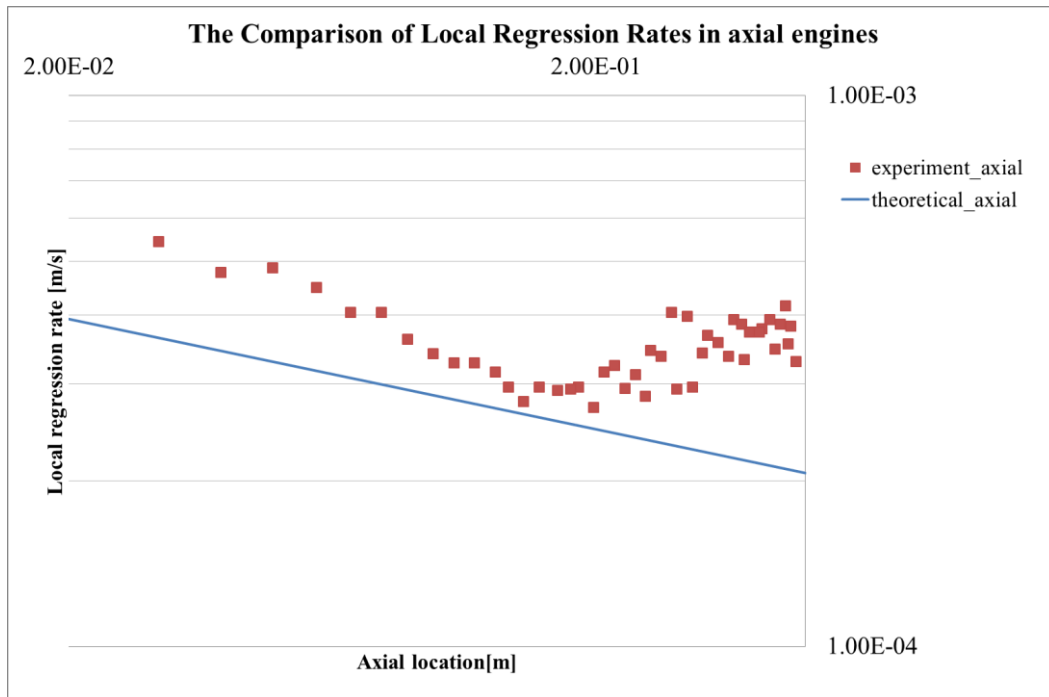


Figure 5. The comparison of the regression rates in axial hybrids between the Marxman's prediction method and the Yuasa's experiment.

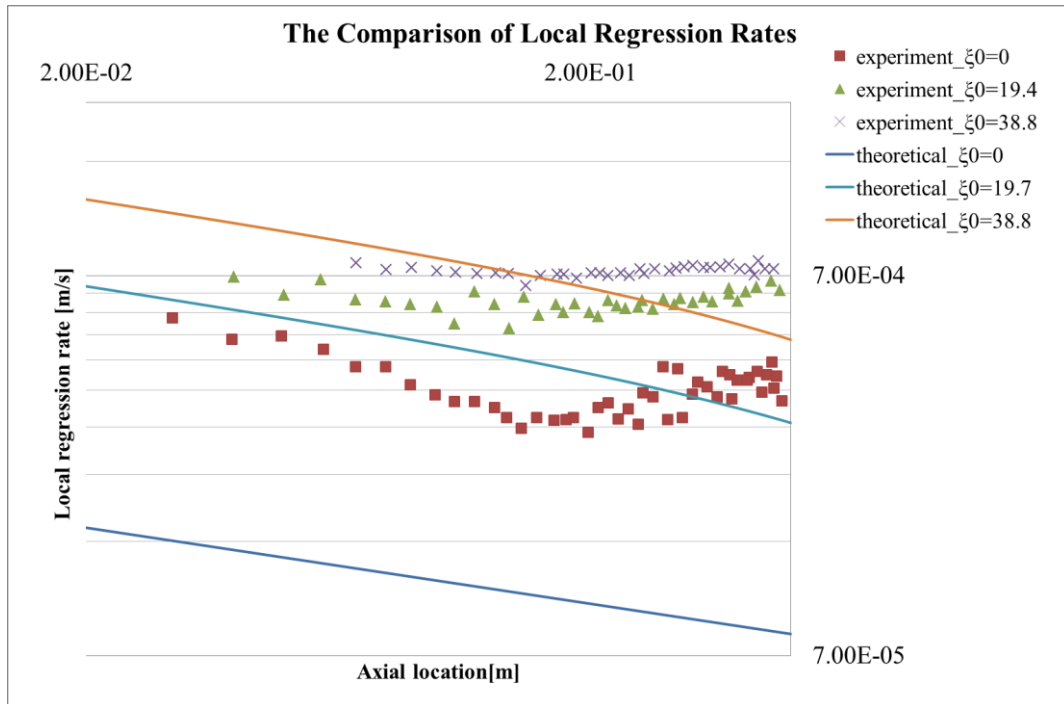


Figure 6. The comparison of the regression rates in swirl hybrids between our theoretical prediction and the Yuasa's experiments.

5. Conclusion

In this paper, we have theoretically reconstructed and extended Marxman's quasi-steady boundary layer combustion model and the prediction method of regression rates in swirling hybrid rocket motors, which has been led by the extension from the two dimensional flat plate boundary layer theory to the three dimensional axisymmetric theory. The derived heat flux equation includes the effect of initial swirl strength and the strengthened fuel blocking effect by swirl. The blocking exponent in strong swirl injections is calculated to be 0.965 in contrast to 0.77 in axial injections. By using this heat flux, eventually, we have derived the equation to evaluate regression rates in swirling hybrid rocket motors.

To confirm the accuracy of this prediction method, we have compared the predicted results with experimental ones by Yuasa et al in two ways. One of them is to compare the representative increase rates of regression rates by swirl through the axial direction with the averaged ones from experiments. Though the assumed flow field seems to be different from experiments to some extent, the estimation of increasing rates is in the same order of magnitude in all swirl strength and is especially well fit in strong swirls. Another one is to compare the predicted local regression rates with experimental data from Yuasa et al. in the both cases of axial and swirl flows. The prediction by the classical theory for axial injection motors constructed by Marxman is compared with the data in the case of axial flow and the result was of the same order of magnitude, however, is not accurate enough to claim the regression rate can be predicted to know the detailed performance. We think the reason for this disagreement is that other effects which increase regression rates such as radiation and the increase of the mass flux by fuel blowing have to be considered. In swirl injection, because the theory derived in this paper is based on the classical one by Marxman et al., the accuracy of the prediction is also low. Therefore, in order to improve the prediction of the local regression rates in swirl injection hybrid motors, we should start from some theoretical correction of Marxman's boundary layer combustion model.

References

- [1] G. Zilliac, and M. A., Karabeyoglu. 2006. Hybrid Rocket Fuel Regression Rate Data and Modeling. In: 42nd AIAA/ASME/SAE/ASEE Joint Propulsion Conference & Exhibit. AIAA 2006-4504.

-
- [2] Yuasa, S., Yamamoto, K., Hachiya, H., Kitagawa, K., and Oowada, Y. 2001. Development of A Small Sounding Hybrid Rocket with a Swirling-Oxidizer-Type Engine. In: *37th AIAA/ASME/SAE/ASEE Joint Propulsion Conference and Exhibit*. AIAA 2001-3537.
- [3] W. H., Knuth, M. J. Chiaverini, J. A., Sauer, and D. J., Gramer. 1998. Solid-Fuel Regression Rate Behavior of Vortex Hybrid Rocket Engines. *Journal of Propulsion and Power*. 18:600-609.
- [4] A., Yoshizawa, H., Abe, H., Fujiwara, Y., Mizobuchi, and Y., Matsuo. 2009. Reynolds-Averaged Modeling of Turbulent-Diffusion Suppression Mechanism in a Swirling Flow. In: *41st Fluid Dynamics Conference / Aerospace Numerical Simulation Symposium*. 23-26.
- [5] Marxman, G. A., and Gilbert, M. 1963. Turbulent Boundary Layer Combustion in the Hybrid Rocket. In: *Symposium (International) on Combustion*. 9: 371–383.
- [6] Marxman, G. A. 1965. Combustion in the Turbulent Boundary Layer on a Vaporizing Surface. In: *Symposium (International) on Combustion*. 10: 1337-1349
- [7] Lees, L. 1958. Convective Heat Transfer with Mass Addition and Chemical Reactions. *Third AGARD Combustion and Propulsion Colloquium*. 451.
- [8] Steenbergen, W. 1995. Turbulent Pipe Flow with Swirl. Ph. D thesis. University Eindhoven of Technology.
- [9] Kito, M., Fujiwara, H., and Nakabayashi, K. 1985. The Direct Measurement of the Shear Stresses in Swirl Pipe Flows. In: *Transactions of the Japan Society of Mechanical Engineers, Series B*. 51:2597-2605.
- [10] M. A., Karabeyoglu, and D., Altman. Transient Behavior in Hybrid Rockets. In: *33rd Joint Propulsion Conference and Exhibit*. AIAA 97-2937.
- [11] G. A., Marxman, C. E., Wooldridge, and R. J., Muzzy. 1963. Fundamentals of Hybrid Boundary Layer Combustion. In: *Heterogeneous Combustion Conference*. AIAA 63-505.
- [12] Czernuszenko, W., and Rylov, A. A. 2000. A Generalization of Prandtl's Model for 3D Open Channel Flows In: *Journal of Hydraulic Research*. 38:173–383
- [13] Dorrance, W. H., and Dore, F. J. 1954. The Effect of Mass Transfer on the Compressible Turbulent Boundary-Layer Skin Friction and Heat Transfer. In: *Journal of the Aeronautical Sciences*. 21:404-410.
- [14] M. A., Karabeyoglu, and D., Altman. 1999. Dynamic Modeling of Hybrid Rocket Combustion. *Journal of Propulsion and Power*. 15:562-571.
- [15] G. A., Marxman. 1967. Boundary-Layer Combustion in Propulsion. *Symposium (International) on Combustion*. 11:269-289.
- [16] Motoe, M., and Shimada, T. 2009. Head-end Injected Swirling Gas Flow in a Chamber In: *45th AIAA/ASME/SAE/ASEE Joint Propulsion Conference & Exhibit*. AIAA 2009-5025.
- [17] Ozawa, K. and Shimada, T. 2013. A theoretical Study in the Skin-friction Coefficient in Swirl Pipe Flows. *ISAS proceedings of Space Propulsion Symposium FY2012*. STCP-2012-070. (Japanese)